Closed-Loop Kinematic Calibration of the Sarcos Dextrous Arm

Lydia Giugovaz and John M. Hollerbach

Biorobotics Laboratory, McGill University
3775 University St., Montreal, Quebec H3A 2B4

Abstract

Closed-loop kinematic calibration has been experimentally implemented on the Sarcos Dextrous Arm. The elbow joint is made mobile by adding an unsensed hinge joint at the endpoint attachment to ground. The calibrated parameters include the joint angle offsets and the hinge-related parameters.

1 Introduction

In the past, we proposed the closed-loop kinematic calibration method [3], which permits a manipulator to be calibrated without endpoint sensing. In this method, a manipulator forms a mobile closed kinematic chain by attachment of the end effector to the environment. This attachment may be rigid or may have up to 5 unsensed degrees of freedom. By placing such a constrained manipulator into a number of poses, the kinematic parameters may be calibrated using joint angle sensing alone and the loop closure equations.

This paper presents an experimental implementation of closed-loop kinematic calibration on the Sarcos Dextrous Arm, a 7-DOF redundant manipulator [11]. With rigid attachment of the endpoint to the environment, the Sarcos Dextrous Arm will form a mobile closed kinematic chain with 1 DOF. Unfortunately, this anthropomorphic arm will have an immobile elbow joint during this motion. In order to make this joint mobile, and hence to identify the parameters associated with this joint, it is necessary to free at least one of the end effector constraints. One way is to add an external unsensed hinge joint; this situation was analyzed in [3] and a procedure was given to eliminate the hinge joint angle from the loop closure equations.

In addition, it is necessary to define a force control strategy, which permits manipulator pose changes in compliance with a constrained end effector and initially incorrect kinematic parameters. In a previous implementation on the fingers of the Utah/MIT Dextrous Hand [2], the fingers were manually placed into different poses and advantage was taken of the backdrivability of the finger joints. For the Sarcos Dextrous Arm, which is a hydraulic manipulator, an active force control strategy is required to move the joints.

In the present paper we are determining only the joint angle offsets and the hinge related parameters, because our main purpose is recalibration of the joint angle offsets. That is to say, we presume that the geometric parameters are already well enough known from the manufacturer's specifications or from previous calibrations. Joint angle offset recalibration is required because of the use of analog sensing at the wrist joints and incremental encoders in the arm joints.

1.1 Related Research

Other researchers have implemented closed-loop calibration, under diverse endpoint constraints. In [14], a line constraint was defined by a laser, which was tracked using an endpoint retroreflector on a PUMA 560 and a 4-quadrant detector. In [5], a fiducial point on the end effector is touched to a fiducial point on the environment in several different poses; this corresponds to the point contact case in [3]. In [12], a teleoperated excavator with unsensed joints was calibrated by adding an additional linkage (called a calibrator by the authors) with some sensed joints to form a closed loop. In [7], a ball bar with fixed length and unsensed spherical joints at each end was employed. Closed-loop calibration of a manipulator with a camera mounted on an end effector was presented in [17].

In the following, we first review open-loop kinematic calibration, then derive closed-loop kinematic calibration using a hinge joint. Experiments on the Sarcos Dextrous Arm are then presented.

2 Methodology

The Denavit-Hartenberg (D-H) convention is employed for the geometric parameters (Figure 1). In the present case, Hayati coordinates are not required because the Sarcos Dextrous Arm has all neighboring joints orthogonal. The subsequent development is taken from [3].

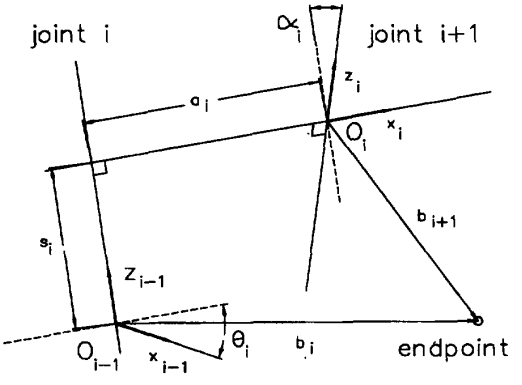

Figure 1: Denavit-Hartenberg coordinates and tip vector b_j^i

2.1 Open-Loop Kinematic Calibration

For a manipulator with n DOFs, the end-effector is located by the position vector $\mathbf{p}_c^i$ and the orientation matrix $\mathbf{R}_c^i$:

$$\mathbf{p}_c^i = \sum_{j=1}^{n} s_j \mathbf{z}_{j-1}^i + a_j \mathbf{x}_j^i \tag{1}$$

$$\mathbf{R}_c^i = \prod_{j=1}^{n} \mathbf{R}_z(\theta_j^i)\mathbf{R}_x(\alpha_j^i) \tag{2}$$

where $\mathbf{R}_z(\phi)$ and $\mathbf{R}_x(\phi)$ are 3-by-3 rotation matrices about the $\mathbf{z}$ and $\mathbf{x}$ axes by the angle ϕ. The subscript c indicates that the position and orientation are computed from the model. The superscript i indicates the configuration of the manipulator. In kinematic calibration, the manipulator must be placed into m poses, with $\boldsymbol{\theta} = [\theta_1^i, \ldots, \theta_n^i]^T$, $i = 1, \ldots, m$, for n links.

The required geometric parameters are s_j, a_j, and α_j for links $j = 1, \ldots, n$. We will model only the joint angle offset θ_j^{off}, related to the actual θ_j' and measured θ_j DH joint angles by the relation $\theta_j' = \theta_j + \theta_j^{off}$. For the calibration, we use a single vector which holds all the unknown kinematic parameters $\boldsymbol{\varphi} = [\boldsymbol{\theta}^{off}, \boldsymbol{\alpha}, \mathbf{s}, \mathbf{a}]^T$, where $\mathbf{s} = [s_1, \ldots, s_n]^T$, etc.

Instead of the orientation matrix $\mathbf{R}_c^i$, it is convenient to represent the orientation by the vector or $\boldsymbol{\rho}_c^i = [\phi_x^i, \phi_y^i, \phi_z^i]^T$, representing the roll-pitch-yaw (ZYX) Euler angles: $\mathbf{R}_c^i = \mathbf{R}_z(\phi_z^i)\mathbf{R}_y(\phi_y^i)\mathbf{R}_x(\phi_x^i)$. The computed endpoint location can than be written as $\mathbf{x}_c^i = [\boldsymbol{\rho}_c^i, \mathbf{p}_c^i]^T$ and given by :

$$\mathbf{x}_c^i = f(\boldsymbol{\theta}^i, \boldsymbol{\varphi}) \tag{3}$$

where the function f is derived from (1) and (2).

To estimate $\boldsymbol{\varphi}$, the manipulator must be put into an adequate number m of configurations, in consideration of the large number of parameters in $\boldsymbol{\varphi}$ and of statistical averaging. At each configuration i, the actual endpoint location $\mathbf{x}_a^i$ is measured. The goal is to determine the $\boldsymbol{\varphi}$ that best predict from the kinematic model (3) all of the endpoint measurements $\mathcal{X} = [\mathbf{x}_a^1, \ldots, \mathbf{x}_a^m]^T$:

$$\mathcal{X} = \mathcal{F}(\boldsymbol{\varphi}) \tag{4}$$

where $\mathcal{F}(\boldsymbol{\varphi}) = (\mathbf{f}(\boldsymbol{\theta}^1, \boldsymbol{\varphi}), \ldots, \mathbf{f}(\boldsymbol{\theta}^m, \boldsymbol{\varphi}))$.

Solving for $\boldsymbol{\varphi}$ from (4) is a nonlinear estimation problem that can be done by linearization and iteration of :

$$\Delta\mathcal{X} = \mathcal{C}\Delta\boldsymbol{\varphi} \tag{5}$$

where $\mathcal{C} = \partial\mathcal{F}/\partial\boldsymbol{\varphi}$. The vector $\Delta\mathcal{X} = [\Delta\mathbf{x}^1, \ldots, \Delta\mathbf{x}^m]^T$, with $\Delta\mathbf{x}^i = \mathbf{x}_a^i - \mathbf{x}_c^i$, contains the location errors. The error in the total parameters is $\Delta\boldsymbol{\varphi} = \boldsymbol{\varphi} - \boldsymbol{\varphi}_0$, where $\boldsymbol{\varphi}_0$ is the current estimate, $\boldsymbol{\varphi}$ is the corrected estimate. In $\Delta\boldsymbol{\varphi}$, $\Delta\mathbf{s} = \mathbf{s} - \mathbf{s}_0$, etc.

An estimate of the parameter errors is provided by minimizing the least-squares function $LS = (\Delta\mathcal{X} - \mathcal{C}\Delta\boldsymbol{\varphi})^T(\Delta\mathcal{X} - \mathcal{C}\Delta\boldsymbol{\varphi})$, which yields

$$\Delta\boldsymbol{\varphi} = (\mathcal{C}^T\mathcal{C})^{-1}\mathcal{C}^T\Delta\mathcal{X}. \tag{6}$$

Finally, the guess at the parameters is updated as $\boldsymbol{\varphi} = \boldsymbol{\varphi}_0 + \Delta\boldsymbol{\varphi}$ and the iteration continues until $\Delta\mathcal{X} \to 0$.

The basis for linearization is the assumption that $\mathbf{x}_c^i$ is close to $\mathbf{x}_a^i$. Then

$$\Delta\mathbf{x}^i = \mathbf{x}_a^i - \mathbf{x}_c^i = \begin{bmatrix} \Delta\boldsymbol{\rho}^i \\ \Delta\mathbf{p}^i \end{bmatrix} \tag{7}$$

where $\Delta\mathbf{p}^i = [dx^i, dy^i, dz^i]^T$ is the incremental position error, and $\Delta\boldsymbol{\rho}^i = [\partial\phi_x^i, \partial\phi_y^i, \partial\phi_z^i]^T$ is the incremental orientation error in term of the Euler angles.

Using differential rotation about orthogonal axis rather than non-orthogonal Euler angles, we have $\Delta\mathbf{r}^i = [\partial x^i, \partial y^i, \partial z^i]^T$. The relation between both are given in [3]. The Jacobians are then found by screw axis analysis as in [3].

2.2 Closed-Loop Calibration with Fixed Endpoint

We next consider a redundant manipulator ($\geq$ 7 DOFs) with fixed end-point. Generally, the resulting closed-loop chain will be mobile, since the fixed endpoint constraints only 6 of the 7 DOFs of the manipulator. We can set the reference frame to be at the fixed endpoint and to have zero orientation and position. Hence $\mathbf{x}_a^i = \mathbf{0}$, and no measurements are required because the actual position is known and is zero by definition.

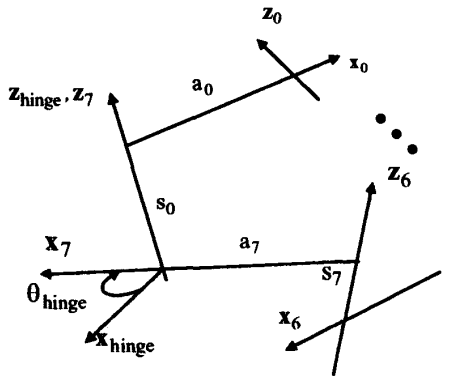

Figure 2: Coordinate description of arm and hinge.

Using the previous mathematical development with one modification, we can write:

$$\Delta \mathbf{x}^i = -\mathbf{x}_c^i = -[\partial x_c^i, \partial y_c^i, \partial z_c^i, dx_c^i, dy_c^i, dz_c^i]^T \quad (8)$$

where $-\Delta \mathbf{r}^i = (\partial x_c^i, \partial y_c^i, \partial z_c^i)$ is the computed orientation, and $-\Delta \mathbf{p}^i = (dx_c^i, dy_c^i, dz_c^i)$ is the computed position. Because the "measured" angles are defined as zero, differential rotation around non-orthogonal Euler axis is equivalent to differential rotation around orthogonal axis. Thus, for the closed-loop case, we have $\Delta \boldsymbol{\rho}^i = \Delta \mathbf{r}^i$.

For the positional component of the loop closure equations, we have

$$\mathbf{p}_c^i = \sum_{j=1}^{n} s_j \mathbf{z}_{j-1}^i + a_j \mathbf{x}_j^i = \mathbf{0}. \quad (9)$$

Ordinarily in the closed-loop procedure this equation is a problem, because the length parameters are linearly dependent. To proceed, it is necessary to specify one length parameter to scale the system size. This is not a problem for the present case, since the manipulator link lengths are presumed known.

2.3 Closed-Loop Calibration with a Hinge Joint

To make the elbow joint mobile, we add a passive, unsensed 1-DOF rotary hinge joint. The hinge is defined to be the -1 joint, with z_{-1}^i positioned along the hinge axis (Figure 2). The endpoint coordinates being arbitrary, it is convenient to make the last joint z_n^i coincident with the hinge axis z_{-1}^i. The hinge coordinates origin can then be positioned at the endpoint coordinates origin.

The geometric parameters needed to define this added unsensed DOF are s_0, a_0, and α_0, defined from hinge coordinates -1 to the manipulator base 0, and s_1. We also need to calibrate the parameters between coordinate 6 and 7: α_7, s_7, and a_7. The hinge angle $\theta_z^i = -\theta_0^i$ measured about z_{-1}^i is unknown and must be eliminated from the 6 kinematic loop closure equations. All other parameters related to the arm are known from the manufacturer's specifications.

To apply the method from hinge to endpoint, we have the position vector, $\mathbf{p}_c^i = \mathbf{0}$ from (9) and $\Delta \mathbf{p}^i = [dx^i, dy^i, dz^i]^T$ from (7), and the endpoint orientation matrix $\mathbf{R}_c^i$ and $\mathbf{R}_{tot}^i$:

$$\begin{aligned} \mathbf{R}_{tot}^i &= \mathbf{R}_z(\theta_0^i)\mathbf{R}_x(\alpha_0^i)\cdots\mathbf{R}_z(\theta_7^i)\mathbf{R}_x(\alpha_7^i) \\ &= \mathbf{R}_x(\partial x^i)\mathbf{R}_y(\partial y^i)\mathbf{R}_z(\partial z^i) \simeq \mathbf{I}_3 \end{aligned} \quad (10)$$

$$\mathbf{R}_c^i = \mathbf{R}_x(\partial x^i)\mathbf{R}_y(\partial y^i)\mathbf{R}_z(\theta_z^i) \quad (11)$$

where $\mathbf{I}_3$ is the 3-by-3 identity matrix, $\mathbf{R}_{tot}^i$ is the total rotation, including the unsensed hinge joint angle, $\mathbf{R}_c^i$ is the total rotation, excluding the hinge joint, ∂x^i and ∂y^i are infinitesimal rotation along axis x and y and θ_z^i is finite rotation along axis z of the coordinates frame -1.

From equations (10) and (11), and using the fact that infinitesimal rotations are commutative, we have that $\mathbf{R}_z(\theta_z^i) = \mathbf{R}_z^T(\theta_0^i)$, or $(\theta_0^i) = -(\theta_z^i)$.

Then, from equations (10) and (11), to solve for the hinge joint, we have :

$$\begin{aligned} \mathbf{R}_c^i &= \left(\mathbf{R}_x(\alpha_0^i)\mathbf{R}_z(\theta_1^i)\cdots\mathbf{R}_z(\theta_7^i)\mathbf{R}_x(\alpha_7^i)\right)^T \\ &= \begin{bmatrix} cos(\theta_z^i) & -sin(\theta_z^i) & \partial y^i \\ sin(\theta_z^i) & cos(\theta_z^i) & -\partial x^i \\ \cdots & \cdots & 1 \end{bmatrix} \end{aligned} \quad (12)$$

or, $\theta_z^i = atan2(\mathbf{R}_{c(2,1)}^i, \mathbf{R}_{c(1,1)}^i)$, where the indices denote the elements of the rotation matrix $\mathbf{R}_c^i$.

The desired variation ∂x^i and ∂y^i are extracted from $\mathbf{R}_c^i\mathbf{R}_z(\theta_z^i) = \mathbf{R}_x(\partial x^i)\mathbf{R}_y(\partial y^i)$. The computed endpoint location is then given, along the hinge base frame (frame -1) by :

$$\Delta \mathbf{x}^i = [\partial x^i, \partial y^i, dx^i, dy^i, dz^i]^T \quad (13)$$

The equations (10) and (13) imply that everything is calculated with respect to the hinge -1 frame. Therefore, to carry on the calibration, the procedure is as follows : calculate the total rotation, without the hinge angle (12) with respect to the base manipulator frame (0 coordinates); extract θ_z^i from (12) and ∂x_c^i, ∂y_c^i from $\mathbf{R}_c^i\mathbf{R}_z(\theta_z^i)$;

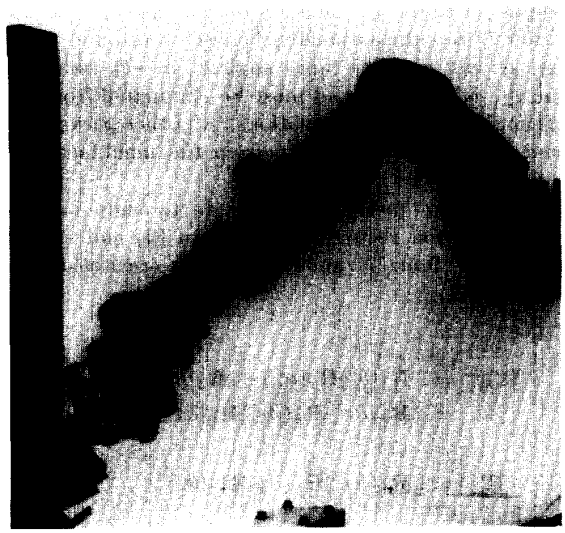

Figure 3: Sarcos Dextrous Arm and hinge joint.

rewrite (10) with respect to hinge joint frame (-1 coordinates); then calculate endpoint position $\Delta\mathbf{p}^i = -\mathbf{p}_c^i$ with respect to the hinge frame.

Since z_{-1}^i aligns with the hinge joint and with z_n^i, then θ_0^{off} can be arbitrarily set to zero. To reflect the reduced dimension of $\mathbf{x}_c^i$, the function $\mathcal{F}$, the vector $\mathcal{X}$, and Jacobian matrix $\mathcal{C}$ are redefined in (4), and (5) by eliminating the third row at each pose. To proceed with the calibration procedure, $\boldsymbol{\varphi}$ is adjusted by keeping the angles offset parameters $(\theta_1^i, \ldots, \theta_7^i)$, and the hinge related ones $(\alpha_0, \alpha_7, s_0, s_1, s_7, a_1, a_7)$. The Jacobian matrix $\mathcal{C}$ is redefined by keeping the columns corresponding to parameters in $\boldsymbol{\varphi}$.

3 Experimental Results

For the first 5 joints of the Sarcos Dextrous Arm, joint angles are sensed by 400,000 count optical encoders. For the last two wrist joints, joint angles are sensed by rotary variable differential transformers (RVDTs) which are sampled by 12-bit ADCs. The manufacturer specifies a linearity of 2% of full scale of a best fit straight line; in addition we observe a noise level of 2 bits.

A fixture was made which rigidly attached the base of the hinge joint to the arm's last link and the hinge beam to the robot mounting table (Figure 3). The location of the hinge joint relative to the arm and to the mounting base was selected such as to have a range of motion wide enough for all the joints, and to have a generated pose set for which the numerical calibration procedure is well conditioned. For example, the hinge joint was positioned such that neither joint 7 nor joint 1 were parallel to it. (Parallel adjacent joints would require Hayati parameters during a numerical calibration [9]).

The following force control strategy was used to move the constrained arm. With rigid attachment of the endpoint to the environment through a hinge joint, the redundant Sarcos Dextrous Arm with 7 DOFs will form a mobile closed kinematic chain with 2 DOFs. Each joint of the Sarcos Dextrous Arm can be controlled via a force control loop (called free mode) or a combined position and force control loop (called position mode). Hence, to move the manipulator in a closed-loop fashion, we set two joints in a position mode, and the remaining ones in a free mode. The joints were chosen experimentally by the ones leading to the most internal motion of the remaining joints.

To improve the numerical performance, we should consider task variable scaling and parameter variable scaling. In a least-squares analysis on the endpoint pose error, position errors and orientation errors have to be combined. It has been argued that for arm lengths of around one meter, then the units of meters and radians are directly comparable [10]. Hence task variable scaling is not performed. Column scaling is performed for the parameters [13]. With regard to identifiability and pose selection, after scaling and for the experiment done and the pose set selected, we obtained a condition number of 28. Scaled condition numbers below 100 are considered acceptable [15].

The results from the closed-loop method, calibrating only for the angle offsets θ_j^{off} and the hinge related parameters, are presented in Table 2. The manufacturer's values are given in Table 1.

At the moment, we have not implemented an independent test to verify the identified parameters. In the mean time, we present the standard deviation of the final pose errors as a measure of goodness of fit. By definition, the "measured" position and orientation from the hinge joint to the end-effector is zero. The standard deviation of the endpoint position is:

$$\sigma_{pos} = \frac{1}{3N}\sqrt{\sum_{i=1}^{m}((x_c^i)^2 + (y_c^i)^2 + (z_c^i)^2)} \qquad (14)$$

where x_c^i, etc., are the computed position components from the identified parameters. The orientation standard deviation is calculated from ∂x^i and ∂y^i only:

$$\sigma_{ori} = \frac{1}{2N}\sqrt{\sum_{i=1}^{m}((\partial x^i)^2 + (\partial y^i)^2)} \qquad (15)$$

j	a_j^m (m)	s_j^m (m)	α_j^m (deg)	θ_j^{off} (deg)
1	0.000	*	90.0	*
2	0.000	0.000	-90.0	*
3	0.000	0.355	90.0	*
4	0.000	0.000	-90.0	*
5	0.000	0.320	90.0	*
6	0.000	0.000	-90.0	*
7	*	*	*	*

Table 1: D-H parameters according to manufacturer's specifications, and to hinge joint location.

For our experiment, we obtained a position standard deviation $\sigma_{pos} = 2.7mm$ and an orientation standard deviation $\sigma_{ori} = 6.6mrad$.

4 Discussion

We have presented experimental results for the closed-loop calibration method applied to the Sarcos Dextrous Arm. The main advantage of this method is that no external sensor device is needed for the calibration. To implement this method for the Sarcos Dextrous Arm, it was necessary for us to free up one endpoint constraint to make the elbow joint mobile, by adding an unsensed passive hinge joint. We also implemented a force control strategy which identified two drive joints and servoed other dependent joints to zero torque.

The errors in the calibrated parameters could be explained by several sources. First and probably most importantly, the RVDTs at the wrist are not that accurate. We plan to overcome this problem in the future by considering these joints to be unsensed and eliminating them from the loop closure equations. Thus there would be three unsensed freedoms at the endpoint, similar to the case of a ball joint except that the axes will not all intersect. Second, the fixed parameters that were used in Table 1 may not be exact. We plan to employ open-loop calibration [1] to check on these parameters and to verify the closed-loop results. Third, the fixture used is very stiff, but it is more flexible than the arm. It could be that there was imperceptible motion between the hinge joint and the end-effector or between the hinge joint and the mounting table.

Another potential problem is that, compared to open-loop calibration, the closed-loop method generates fewer and more limited poses because the endpoint is fixed. The joint ranges are also smaller. However, with a scaled condition number of 28, it appears that the closed-loop poses were adequate for this identification problem.

j	a_j (m)	s_j (m)	α_j (deg)	θ_j^{off} (deg)
0	0.202	.014	-38.5	n/a
1		.273		9.9
2				-122.8
3				-21.1
4				-9.2
5				27.1
6				116.3
7	-0.101	0.038	99.8	89.3

Table 2: D-H parameters derived from closed-loop method.

Acknowledgements

Support for this research was provided by the Natural Sciences and Engineering Research Council (NSERC) Network Centers of Excellence Institute for Robotics and Intelligent Systems (IRIS). Personal support for JMH was provided by the NSERC/Canadian Institute for Advanced Research (CIAR) Industrial Chair in Robotics and for LG by an NSERC Postgraduate Scholarship.

References

[1] C.H. An, C.G. Atkeson, and J.M. Hollerbach, *Model-Based Control of a Robot Manipulator*. Cambridge, MA: MIT Press, 1988.

[2] D.J. Bennett, and J. M. Hollerbach, "Closed-loop kinematic calibration of the Utah-MIT Hand," *Experimental Robotics 1 — The First International Symposium*, edited by V. Hayward and O. Khatib. N.Y.: Springer-Verlag, pp. 539-552, 1990.

[3] D.J. Bennett and J.M. Hollerbach, "Autonomous calibration of single-loop closed kinematic chains formed by manipulators with passive endpoint constraints," *IEEE Trans. Robotics and Automation*, vol. 7, pp. 597-606, 1991.

[4] D.J. Bennett, J.M. Hollerbach, and D. Geiger, "Autonomous robot calibration for hand-eye coordination," *Intl. J. Robotics Research*, vol. 10, pp. 550-559, 1991.

[5] J.J. Craig, "Calibration of industrial robots," in *Proc. 24th Intl. Symp. on Industrial Robots*, Tokyo, November, 1993.

[6] J. Denavit and R.S. Hartenberg, "A kinematic notation for lower pair mechanisms based on matrices," *J. Applied Mechanics*, vol. 22, pp. 215-221, 1955.

[7] M.R. Driels, "Using passive end-point motion constraints to calibrate robot manipulators," *J. Dynamic Systems, Meas., Control*, vol. 115, pp. 560-565, 1993.

[8] R.V. Dubey, J.A. Euler, and S.M. Babcock, "Real-time implementation of an optimization scheme for seven-degree-of-freedom redundant manipulators," *IEEE Trans. Robotics and Automation*, vol. 7, pp. 579-588, 1991.

[9] S.A. Hayati and M. Mirmirani, "Improving the absolute positioning accuracy of robot manipulators," *J. Robotic Systems*, vol. 2, pp. 397-413, 1985.

[10] J.M. Hollerbach, "Advances in robot calibration," in *6th Intl. Symp. Robotics Research*, Hidden Valley, PA, Oct. 2-5, 1993.

[11] S.C. Jacobsen, F.M. Smith, D.K. Backman, and E.K. Iversen, "High performance, high dexterity, force reflective teleoperator II," in *ANS Topical Meeting on Robotics and Remote Systems*, Albuquerque, NM, Feb. 24-27, 1991.

[12] M. Khoshzaban, F. Sassani and P.D. Lawrence, "Autonomous kinematic calibration of industrial hydraulic manipulators," *Robotics and Manufacturing*, (vol. 4), edited by M. Jamshidi, R. Lumia, J. Mullins, and M. Shahinpoor. NY: ASME Press, pp. 577-584, 1992.

[13] C.L. Lawson and R.J. Hanson, *Solving Least Squares Problems*. Englewood Cliffs, N.J.: Prentice - Hall, pp. 180-198, 1974.

[14] W.S. Newman and D.W. Osborn, "A new method for kinematic parameter calibration via laser line tracking," in *IEEE Intl. Conf. Robotics and Automation*, Atlanta, pp. 2:160-165, May 2-7, 1993.

[15] K. Schroer, L. Uhl, S. Albright, and M Huttenhofer, "Ensuring solvability and analyzing results of the nonlinear robot calibration problem," in *Second International Symposium on Measurement and Control in Robotics*, Tsukuba Science City, Japan, pp. 851-858, 1992.

[16] H.W. Stone, *Kinematic Modeling, Identification, and Control of Robotic Manipulators*. Boston: Kluwer Academic Publ., 1987.

[17] H. Zhuang, L. Wang, and Z. Roth, "Simultaneous calibration of a robot and a hand-mounted camera," in *IEEE Intl. Conf. Robotics and Automation*, Atlanta, pp. 2:149-154, May 2-7, 1993.